RGB Tip distance to the faint gas-rich dwarf KK 153

M. Bellazzini¹, G. Beccari², R. Pascale¹, D. Paris³, F. Annibali¹, F. Cusano¹, and D. Pérez-Millán¹

- ¹ INAF Osservatorio di Astrofisica e Scienza dello Spazio di Bologna, via Piero Gobetti 93/3, 40129 Bologna, Italy
- European Southern Observatory, Karl-Schwarzschild-Strasse 2, 85748 Garching bei München, Germany
- INAF Osservatorio Astronomico di Roma, Via Frascati 33, 00078, Monteporzio Catone, Rome, Italy

Accepted for publication by A&A

ABSTRACT

KK 153 is a star-forming dwarf galaxy that has been recently proposed as a new member of the sparsely populated class of gas-rich ultra faint dwarfs, lying in the outskirts of the Local Group. We used the Large Binocular Telescope under sub-arcsec seeing conditions to resolve for the first time the outer regions of KK 153 into individual stars, reaching the red giant branch. The magnitude of the red giant branch tip was used to measure a distance of $D = 3.06^{+0.17}_{-0.14}$ Mpc, much more accurate and precise than the estimate previously available in the literature, based on the baryonic Tully-Fisher relation ($D = 2.0^{+1.7}_{-0.8}$ Mpc). The new distance places KK 153 clearly beyond the boundaries of the Local Group, and, together with a new measure of the integrated magnitude, implies a stellar mass of $M_{\star} = 2.4 \pm 0.2 \times 10^6 M_{\odot}$. The dwarf populates the extreme low-mass tail of the M_{\star} distribution of gas-rich galaxies but it is significantly more massive than the faintest local gas-rich dwarfs, Leo T and Leo P. In analogy with similar systems, the star formation history of KK 153 may have been impacted by the re-ionisation of the Universe while keeping a sufficient gas reservoir to form new stars

Accepted for publication by A&A

Accepted for publication by A&A

ABSTI

KK 153 is a star-forming dwarf galaxy that has been recently propultra faint dwarfs, lying in the outskirts of the Local Group. We used to resolve for the first time the outer regions of KK 153 into individual giant branch tip was used to measure a distance of $D = 3.06^{+0.17}$ available in the literature, based on the baryonic Tully-Fisher relabeyond the boundaries of the Local Group, and, together with a note of KK 153 may have been impacted by the re-ionisation of the U several Gyr later.

Key words. Galaxies: dwarf – Galaxies: individual: KK 153

1. Introduction

The exploration of the very faint end of the galaxy luminosity function is a fascinating endeavour that can be pursued only in the local Universe, where extremely faint stellar systems can be actually detected (Belokurov 2013; Simon 2019). One of the techniques that has been used in the last decade to look for very faint nearby galaxies, down to the regime of almost dark (Cannon et al. 2015; Giovanelli & Haynes 2015; Sand et al. 2015; Leisman et al. 2017, 2021; Jones et al. 2023) or, possibly, completely dark systems (Anand et al. 2025), has been to search for stellar counterparts of compact H I clouds whose low line-of-sight (los) velocity is compatible with a local nature (see, e.g., Adams et al. 2013; Saul et al. 2014, for recent catalogues of such clouds). Systematic searches led to the discovery of a handful of gas-rich low-mass stellar systems (see, e.g., Cannon et al. 2015; Bellazzini et al. 2015a,b; Sand et al. 2015a), the most intriguing case being probably Leo P, a low-mass very metal-poor star-forming dwarf galaxy at $D \approx 1.6$ Mpc, likely associated with the NGC 3109 group (Giovanelli et al. 2013; Skillman et al. 2013; McQuinn et al. 2015, 2024).

Along this line of research, Xu et al. (2025) recently identified the stellar counterpart of a low-velocity compact H 1

Along this line of research, Xu et al. (2025) recently identified the stellar counterpart of a low-velocity compact H_I cloud discovered in the Five-hundred-meter Aperture Spherical radio Telescope (FAST) extragalactic H1 survey (Zhang et al. 2024). In spatial coincidence with the H_I cloud they found a small bluish galaxy of elongated shape, KK 153 (LEDA 4192). Xu et al. (2025), having carefully analysed all the available data concluded that KK 153 has a stellar mass near the threshold adopted to divide ordinary dwarf galaxies and Ultra Faint Galaxies (UFDs; $M_{\star} \simeq 10^5 M_{\odot}$; McQuinn et al. 2024), thus suggesting that it may be a new member of the rare class of gas-rich UFDs in the Local Group or its immediate vicinity,

together with Leo T (D = 0.4 Mpc Irwin et al. 2007) and Leo P (D = 1.6 Mpc, McQuinn et al. 2015).

However, many of the conclusions drawn by Xu et al. (2025) were based on a highly uncertain distance estimate, based on the baryonic Tully-Fisher relation, $D = 2.0^{+1.7}_{-0.8}$. In our experience, a much more accurate distance measure for dwarfs in this distance range can be very efficiently obtained with less than half an hour of observation with the Large Binocular Camera (LBC, mounted at the Large Binocular Telescope¹; Giallongo et al. 2008) in binocular mode, under sub-arcsec seeing conditions (Bellazzini et al. 2011, 2015a; Annibali et al. 2020; Sacchi et al. 2024), by resolving the outskirts of these galaxies into individual stars to a depth where the tip of the Red Giant Branch (RGB) can be used as a standard candle (see, e.g., Lee et al. 1993; Salaris & Cassisi 1998; Madore & Freedman 2020; Bellazzini & Pascale 2024, and references therein). For this reason we asked to observe KK 153 with LBC under the Italian LBT Director Discretionary Time and we were awarded time under the programme DDT-2024B-03.

In this paper we describe the results of this experiment, that lead to a significantly revised and improved measure of the distance to KK 153. Albeit our new measure locates KK 153 clearly beyond the Local Group, implying a larger stellar mass than that inferred by Xu et al. (2025), KK 153 remains among the least massive local and isolated gas-rich dwarfs, sampling the vicinity of the mass threshold of systems that were able to survive quenching by the background UV radiation field that re-ionised the Universe, a crucial regime to understand the evolution of dwarf galaxies (see, e.g., and references therein Gutcke et al. 2022; Xu et al. 2025; Mutlu-Pakdil et al. 2025; McQuinn et al. 2024; Jones et al. 2025).

¹ LBT; https://www.lbto.org

The paper is organised as follows: in Sect. 2 we describe the observations, the data reduction and calibration, the adopted selection and the Colour Magnitude Diagram (CMD) of KK 153 that we obtained from our data; in Sect. 3 we derive a new distance measure to KK 153 using the RGB Tip as a standard candle and we provide new measures of the integrated magnitudes and estimates of the stellar mass. Finally, in Sect. 4 we summarise and briefly discuss our results. The most relevant properties of KK 153 derived in this paper are summarised in Table 1.

Table 1. Main properties of KK 153.

Parameter	Value	Notes
$(m-M)_0$	$27.43^{+0.12}_{-0.10}$	this work
D	$3.06^{+0.17}_{-0.14}$ Mpc	this work
E(B-V)	0.009 ± 0.001	SFD98+SF10
r_0	16.35 ± 0.14	integrated, t.w.
g_0	16.86 ± 0.09	integrated, t.w.
R_h	$17.4'' \pm 0.8''$	(major axis) this work
M_V	-10.87 ± 0.20	this work
${M}_{\star}$	$2.4 \pm 0.2 \times 10^6 M_{\odot}$	this work
$M_{H_{\rm I}}$	$1.2 \pm 0.4 \times 10^6 M_{\odot}$	t.w. + Xu et al. (2025)
ell = (1 - b/a)	0.4	HyperLeda ^a
PA	$167.0^{\circ} \pm 1.7^{\circ}$	Xu et al. (2025)
V_h	$127.5 \pm 0.2 \text{ km s}^{-1}$	Xu et al. (2025)

Notes. a http://atlas.obs-hp.fr/hyperleda/. V_h is the heliocentric line of sight velocity, measured with H I observations.

2. Observations and data reduction

Observations were carried out with the LBC in binocular mode, providing simultaneous imaging in the Sloan Digital Sky Survey² (SDSS) g and r bands. The data were acquired on May 21, 2025 (UT) under clear sky conditions, with an average seeing of 0.9". The total exposure time per filter was 1800 s, split into six individual 300 s exposures. The images were bias-subtracted, corrected for flat-field and cleaned from hot and dead pixels as well as for cosmic ray hits with the standard procedure adopted by the INAF LBT-Italia team³ (see, e.g., Annibali et al. 2020, for a detailed description). A portion of an image obtained from the stacking of all the g and r images centred on KK 153 is shown in Fig. 1. A population of bright blue stars broadly clustered in the central regions, along the minor axis, is surrounded by an elongated and more extended halo of fainter and redder stars, fully consistent with the findings by Xu et al. (2025).

LBC is a mosaic of four adjacent 4608 px×2048 px CCDs, with a pixel scale of 0.225"px⁻¹ (Giallongo et al. 2008). Each CCD chip covers a field of 17.3'×7.7'. In our images, KK 153 is imaged near the center of the central chip (Chip 2; slightly offset to minimise the contaminating effect of a few very bright stars in the field). Since the field of view of Chip 2 is wide enough to sample KK 153 and an ample portion of the surrounding field, in the following we limit our analysis to Chip 2 images, as done in Bellazzini et al. (2011) in the study of a similar system.

We performed Point Spread Function (PSF) photometry of individual stars using DAOPHOT II (Stetson 1987). In summary, 20 to 30 well-sampled, not saturated and isolated stars were selected in each individual frame to estimate the

PSF models. The best PSF models were fit using a Lorentz function. The spatial trends of the PSF shape within the frame were fitted with a second order polynomial in x,y. The PSF fitting was performed on each image using the ALLFRAME routine (Stetson 1994). We first created a master catalogue of sources selecting the objects with peaks higher than 3σ above the background in a stacked image obtained by registering and co-adding all the images considered for the analysis. Then, ALLFRAMES automatically identifies and fits each of these sources on the individual images. Only sources found at least in three g and three r images were retained in the final catalogue. The average and the standard error of the mean of the independent measures obtained from the different images were adopted as the final values of the instrumental magnitude and of the uncertainty on the relative photometry.

In wide-field deep stellar photometry, distant background galaxies are the major source of contamination (see Bellazzini et al. 2011, for a detailed discussion in a very similar context and for further references). To mitigate the contamination of our sample by these sources and by other spurious detections we adopted the magnitude-dependent selection on the DAOPHOT II SHARP parameter illustrated in the upper panel of Fig. 2^4 . SHARP should take values as near to zero as the shape of the light distribution is more similar to that expected from a point-like source (PSF), while significant deviations toward positive values indicates extended sources (e.g, galaxies or blended stars) and deviations toward negative values identify sources more compact than point sources (like, e.g., residual small cosmic spikes or hot pixels). The adopted selection should remove a large fraction of contaminating background galaxies, with efficiency decreasing toward fainter magnitudes, as expected.

The middle and lower panels of Fig. 2 show the distribution of photometric errors as a function of the magnitude, in r and g. The photometric error is ≤ 0.05 mag for $g(r) \lesssim 25.0(24.0)$, then it gently increases, reaching ≈ 0.2 mag at $g(r) \approx 27.0(26.0)$. To further clean the final catalogue on which we performed the scientific analysis, in addiction to the selection in SHARP described above, we rejected all the sources having $err_g \geq 0.2$ or $err_r \geq 0.2$. The distribution in the sky of the finally selected sources is presented in Fig. 3, where we plot in red the sources within R = 2.0' from the centre of KK 153 (taken from Xu et al. 2025) and in cyan those farther that R = 3.0', as, in the following, these two regions will often serve as reference for the KK 153 "on target" sample and for the Control Field, respectively. The over-density of sources corresponding to the resolved stars in KK 153 is readily evident at the center of the red circular region.

2.1. Photometric and astrometric calibrations

The astrometric and photometric calibrations have been achieved using sources in common with the SDSS-DR16 dataset (Ahumada et al. 2020). The astrometry of our raw catalogue has been mapped into the SDSS-DR16 system with a 4th order polynomial fitted on 112 stars in common, with the appropriate code of CataPack⁵ suite. The resulting rms spread is < 0.15" both in RA and DEC.

https://www.sdss.org

³ https://lbt.inaf.it

⁴ In particular we retain all the sources having r <= 23.0 and |SHARP| < 0.3, or r > 23.0 and |SHARP| < 0.44r - 9.82. The selection window has been drawn by eye to reject most of the obvious outlier of the distribution of SHARP as a function of magnitude, with particular care for the rejection of marginally extended objects.

http://davide2.bo.astro.it/~paolo/Main/CataPack.html

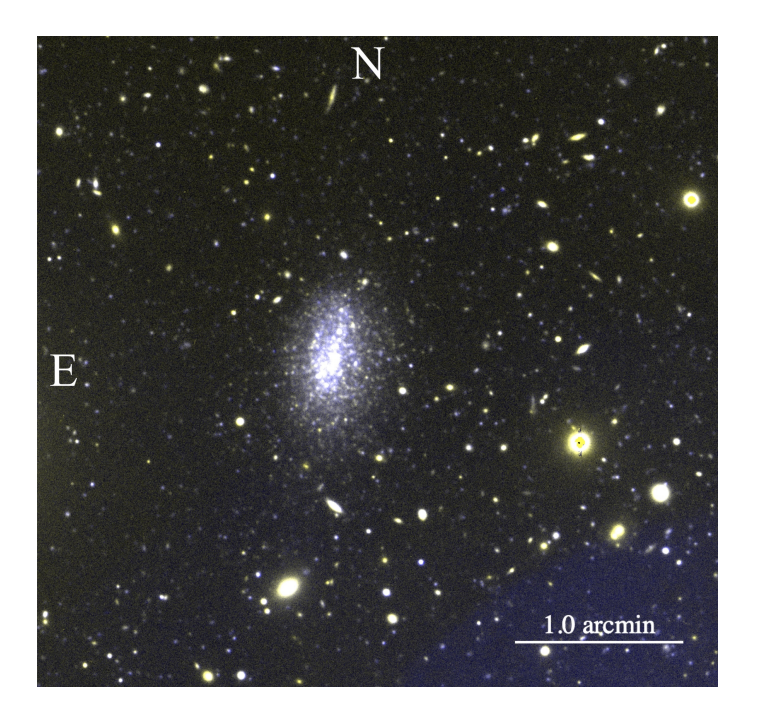


Fig. 1. Red-Green-Blue cut-out image of KK 153 and its immediate surroundings obtained from sky-subtracted, stacked deep g and r images. The r image has been used for both the Red and the Green channels, while the g image has been used for the Blue channel.

The photometric calibration has been obtained from the subset of the brightest sources classified as stars in SDSS-DR16, about 50 stars covering the colour range enclosing the large majority of the stars of scientific interest, $0.0 \le g - r \le 1.8$. A first order polynomial as a function instrumental g-r colour has been adopted, strictly analogous to what done in Bellazzini et al. (2011), Bellazzini et al. (2015a), and Annibali et al. (2020). In the following, the rms spread about the calibrating relations, 0.073 mag and 0.076 mag in g and r band, respectively, will be added in quadrature to the error budget of all the derived quantities that depend on the absolute photometric calibration.

2.2. Surface photometry

We performed the integrated photometry of the galaxy using the Aperture Photometry Tool (APT; Laher et al. 2012a,b) on our stacked g and r images. Having verified that the axis ratio reported in the Hyperleda⁶ catalogue (Makarov et al. 2014) and the position angle reported by Xu et al. (2025) are appropriate for KK 153 (see Table 1), we adopted elliptical apertures accordingly shaped and oriented.

To measure the integrated photometry we adopted an aperture with semi-major axis of 180 px = 40.5'', that should enclose most of the KK 153 light. The sky background was computed on a concentric elliptical annulus with inner(outer) semi-major axis of 300 px(350 px), width=11.25'', wide enough to account for the contribution of background/foreground sources to the surface photometry over such large apertures.

Our integrated magnitudes are $\simeq 0.5$ mag brighter than those reported by Xu et al. (2025). No detail on the way in which their integrated magnitudes have been obtained is reported in Xu et al. (2025). A possible explanation for the observed difference is that they may have adopted a smaller aperture. With the

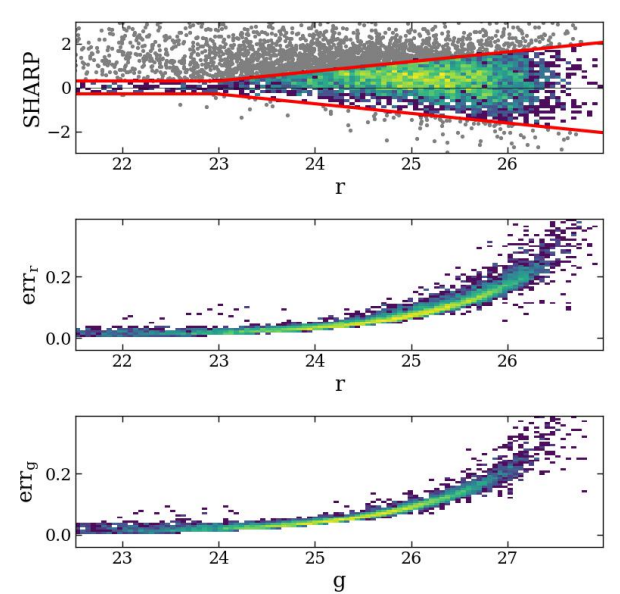


Fig. 2. Upper panel: distribution of the Daophot SHARP shape parameter as a function of r magnitude. Sources lying in the region enclosed by the red contours are considered as likely stars, while those outside the contours (grey points), mostly distant unresolved galaxies, have been excluded from the subsequent analysis. Middle and lower panels: distribution of the photometric errors in r and g as a function of r and g magnitude, respectively.

same aperture used above, we obtain results fully compatible with those from LBC images, within the uncertainties, from photometrically calibrated SDSS images, thus supporting our measures. The rationale behind the choice of a large aperture, was driven by the fact that we detect RGB stars attributable to KK 153 at least out to $R \simeq 1.5'$ from the centre of the galaxy (see below). The finally adopted aperture size is trade-off between the extension of the stellar distribution and the requirement of avoiding the inclusion of an excessively extended region where the light from the galaxy is below the sky level.

Finally, we empirically estimated the half-light radius as the semi-major axis of the elliptical aperture containing half of the flux measured in the aperture used for the integrated magnitude. The value reported in Table 1 is the average of the values we got from the g and r images, the uncertainty is the associated standard deviation.

2.3. The Colour Magnitude Diagram

The CMDs of the sources enclosed within 2.0' (galaxy) and of those lying farther than 3.0' from the centre of KK 153 (field) are shown in the left and middle panels of Fig. 4, respectively. The "field" stars are distributed over a sky area that is more than 8.3 times the area covered by the "galaxy" sample. All the magnitudes are corrected for foreground extinction adopting $A_g = 3.734E(B-V)$ and $A_r = 2.583E(B-V)$, following Bellazzini & Pascale (2024), and E(B-V) = 0.009 from the Schlegel et al. (1998, SFD98) reddening maps recalibrated according to Schlafly & Finkbeiner (2011, SF10). We used the same maps to verify that the extinction variations are negligible across the considered FoV.

⁶ http://atlas.obs-hp.fr/hyperleda/

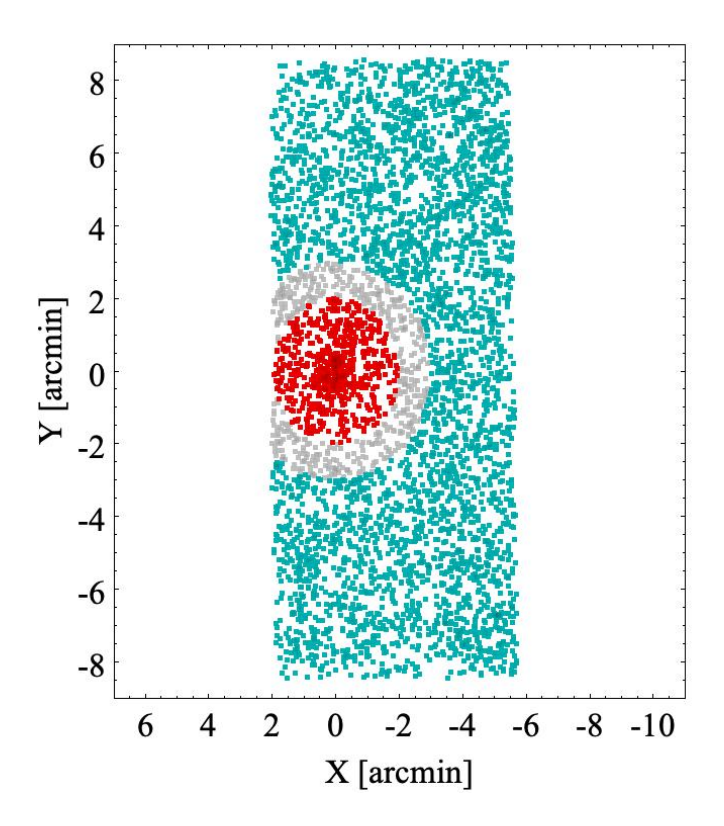


Fig. 3. Sky map of the position of the sources in our selected catalogue, in an orthographic projection reference system with the origin at the center of KK 153. North is up, East to the left. Sources within 2.0' from the centre of KK 153 are plotted in red (galaxy), sources with R > 3.0' are plotted in cyan (field).

For $r_0 \ge 23.5$, the CMD of the field is dominated by the wedge-shaped distribution of distant galaxies in the blue sequence, around $(g-r)_0 \simeq 0.2$, while most of the sources redder than $(g - r)_0 \simeq 1.0$, at any magnitude, are likely local M dwarfs, and most bluer sources at $r_0 \le 23.5$ are Galactic main sequence (MS) stars along the line of sight (Bellazzini et al. 2011). In the R < 2.0'' CMD the blue sequence wedge is still the dominant feature, but a handful of stars bluer than $(g - r)_0 \simeq 0.0$ also emerges, having no counterpart in the field: these are young stars located in the innermost corona of KK 153 that our observations are able to resolve into stars. An over-density of stars in the colour range $0.8 \le (g - r)_0 \le 1.5$ is also apparent, when compared to the "field" CMD. In analogy to the cases shown and discussed by Sacchi et al. (2024) in a very similar context, we identify this wide sequence as the upper RGB of KK 153, tipping about $r_0 \simeq 24.5$. In the right panel of Fig. 4 we illustrate how we selected candidate RGB stars of KK 153 in the following analysis.

However, given the relatively low number of likely KK 153 stars that we actually resolve, before proceeding with the measure of the distance, we want to provide additional evidence that we have indeed positively detected the RGB of the galaxy. The comparison between the colour distribution of the "galaxy", here defined as the R < 1.5' circle to maximise the contrast, and "field" samples in upper panel of Fig. 5, normalised to their areas, clearly shows that in the galaxy there is a strong excess of stars in the range $1.0 \le (g - r)_0 \le 1.5$ with respect to the field. Limiting the comparison to stars fainter than $r_0 = 23.0$, we found that, according to the Kolmogorov-Smirnov test, the

probability that the two distributions are drawn from the same parent population is as low as $P_{KS} = 1.7 \times 10^{-7}$.

Then, selecting the candidate RGB stars as shown in the left panel of Fig. 4, with the additional condition $r_0 > 23.0$, we derive the surface density profile of these stars about the centre of KK 153, along the major axis, using the elliptical radius R_{ell} as defined in Eq. 1 of Perina et al. (2009). The profile, shown in the lower panel of Fig. 5, demonstrate that the stars that we identify as RGB members of KK 153 are highly over-dense around the centre of the galaxy and are distributed along a coherently declining profile, over a scale of 4-5 half light radii⁷. The difference in the surface density of RGB stars between the R < 1.5(2.0)' and the R > 3.0' regions exceeds zero by more than $8.6\sigma(8.3\sigma)$. Hence, there is no doubt that we have resolved the brightest ≈ 2 mag of the RGB of KK 153.

3. Distance and stellar mass

To measure the magnitude of the RGB Tip of KK 153 we apply the bayesian inference model described in Bellazzini & Pascale (2024) to the colour-selectd RGB stars lying within 2.0' from the centre of the galaxy. The actual detection is illustrated in Fig. 6, giving $r_0^{TRGB} = 24.51_{-0.06}^{+0.08}$.

Bellazzini & Pascale (2024) do not provide a calibration of M_r^{TRGB} , since the relatively blue r band is not ideal to trace the tip over a large range of metallicity / RGB colours. However, here we are dealing with low-mass, metal-poor populations, that is a regime where M_r^{TRGB} depends only very weakly on colour (Bellazzini et al. 2011). Moreover, we derive the distance modulus taking as reference the RGB Tip of the Small Magellanic Cloud (SMC), that has a mean tip colour similar to KK 153 ($(g-r)_0^{TRGB}=1.13$, and $(g-r)_0^{TRGB}=1.22$ for KK 153 and the SMC, respectively). Using the same sample and the same technique as Bellazzini & Pascale (2024) we obtained for the SMC $M_r^{TRGB}16.080 \pm 0.022$. Adopting $(m-M)_0^{SMC}=18.997 \pm 0.032$ from Graczyk et al. (2020), we obtain $M_r^{TRGB}=-2.917 \pm 0.039$ for SMC-like RGB populations, in reasonable agreement with the value derived by Bellazzini et al. (2011) for $(g-r)_0^{TRGB}<1.4$ from theoretical models.

If we take the SMC as our distance reference, the distance modulus $(m - M)_0 = 27.43^{+0.12}_{-0.10}$ is obtained for KK 153, including the uncertainty in the photometric calibration. This corresponds to $D = 3.06^{+0.17}_{-0.14}$ Mpc, with uncertainties reaching $^{+0.22}_{-0.20}(^{+0.33}_{-0.31})$ Mpc if an additional uncertainty of 0.1(0.2) magnitudes for the TRGB calibration in r band is hypothesised.

There is no sound way to estimate the amount of any systematic uncertainty possibly associated to the adopted calibration. As a broad reference we can note that, e.g., a shift of 0.08 mag is required to match the predictions from the PARSEC (Bressan et al. 2012) models with the adopted measure of $M_{I_E}^{TRGB}$ for the SMC and that the scatter of those models at the colour of the SMC due to an age spread of 9 Gyr is < 0.04 mag (Bellazzini & Pascale 2024). The exercise performed here by considering 0.1 mag and 0.2 mag additional uncertainty is meant to show that the 1σ accuracy of our distance measure remains below $\approx 10\%$ also when an unrealistically large uncertainty on the calibration is assumed.

In Fig. 7 we compare the observed CMD of KK 153 with a set of theoretical isochrones from the PARSEC dataset (Bressan

⁷ The drop of the surface density in the innermost point is due to the strong incompleteness affecting the central, overcrowded regions of the galaxy in our images.

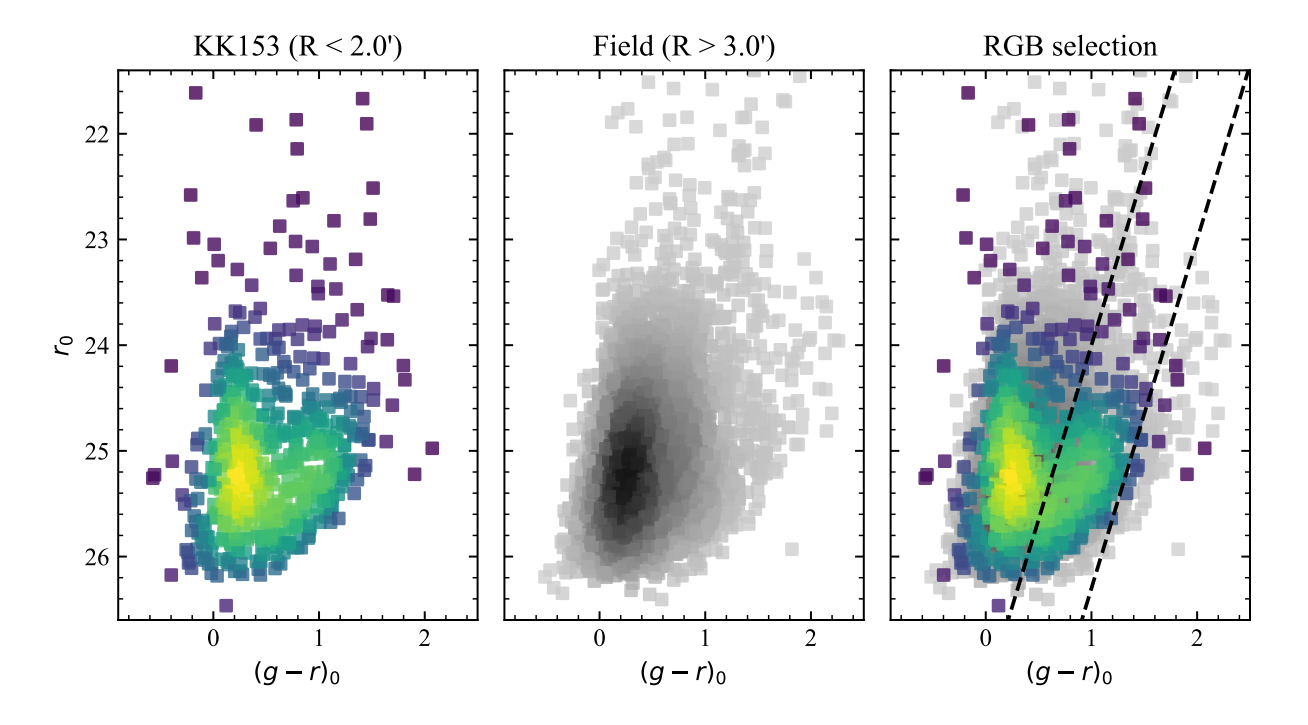


Fig. 4. Left panel: CMD of stars enclosed within a circle of radius=2.0' centred on the center of KK 153. Middle panel: CMD of all the stars in our field located at an angular distance larger than =3.0' from the centre of KK 153 (Field). It is worth noting that the area of the R > 3.0' field is more than 8.3 times the area of the R < 2.0' circle around the galaxy. Right panel: the CMD of KK 153 superimposed to the CMD of the Field population. The two dashed parallel lines display our selection of candidate RGB stars of KK 153. In all the CMDs the colour intensity of the points is proportional to the local star count density (Hess diagram).

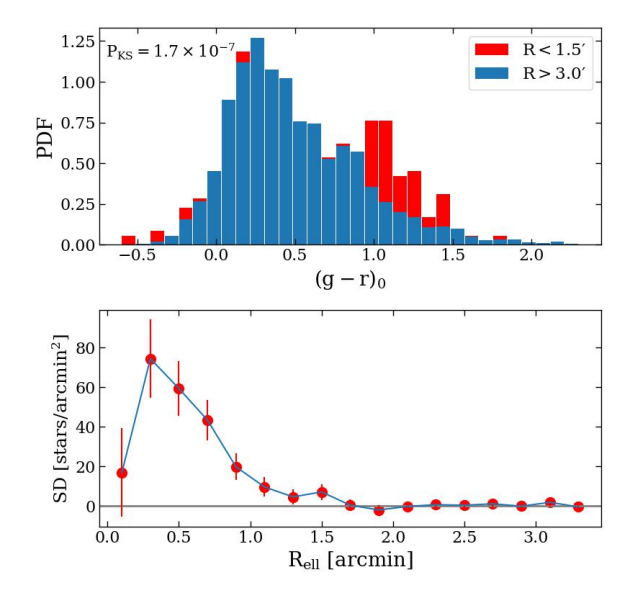


Fig. 5. Upper panel: the colour distribution of the stars within 1.5′ from the centre of KK 153 (red histogram) is compared to the colour distribution of the Field stars (R > 3.0′; blue histogram). Lower panel: background-subtracted surface density profile of RGB stars (selected as in Fig. 4, with the additional condition $r_0 > 23.0$) from the centre of KK 153.

et al. 2012, obtained with the dedicated web tool⁸) shifted to

our newly derived distance (D=3.06 Mpc, left panel) and to the distance inferred by Xu et al. (2025, D=2.0 Mpc, right panel). The short distance assumption clearly fails to match the observed RGB. On the other hand, for D=3.06 Mpc the bundle of isochrones spanning the metallicity $-2.0 \le [M/H] \le -1.0$ and the age range 5-10 Gyr provides a fully satisfactory fit of the observed RGB. The handful of Main Sequence and Blue Loop stars that we were able to resolve are well matched by [M/H] = -1.0 isochrones of age 40 Myr and 63 Myr, suggesting that the star formation was active until very recent epochs in KK 153, possibly still ongoing.

The derived distance locates KK 153 significantly farther away than the estimate by Xu et al. (2025), clearly beyond the boundaries of the Local Group, and reduces the uncertainties from more than 50% to less than 10%. Indeed, Fig. 8 shows that KK 153 is located between the M81 and the CVn I galaxy groups, and, similarly to the other recently-discovered gas-rich low-stellar-mass dwarfs discussed in Mutlu-Pakdil et al. (2025), is remarkably isolated. The nearest confirmed galaxy in the Pace (2024, P24 hereafter) catalogue is UGC 8508 at 630 kpc, itself a pretty isolated dwarf.

3.1. Stellar mass

The distance modulus derived above was used to convert apparent integrated magnitudes into their absolute counterparts $M_g = -10.57 \pm 0.15$ and $M_r = -11.08 \pm 0.15$. $M_V = -10.87 \pm 0.20$ was obtained with the photometric transformation

$$V = g - 0.5784(g - r) - 0.0038 \tag{1}$$

⁸ https://stev.oapd.inaf.it/cgi-bin/cmd

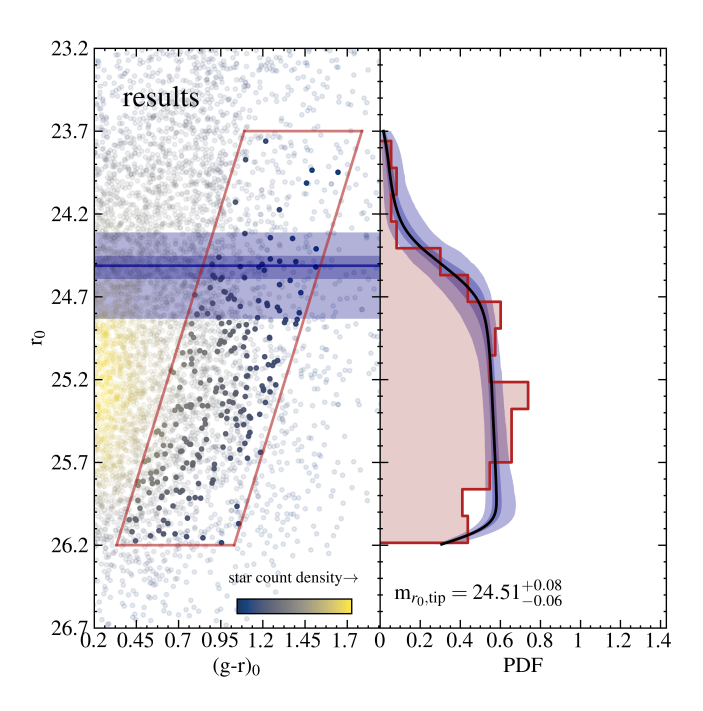


Fig. 6. Measure of the RGB Tip following Bellazzini & Pascale (2024). Left panel: CMD zoomed on the RGB of KK 153, with the stars colour coded according to the local star count density. The red polygon displays the selection window of the stars used for the detection of the tip, with the additional constraint R < 2.0'. The horizontal line marks the position of the tip, while the dark purple and light purple bands mark the $\pm 1\sigma$ and $\pm 3\sigma$ uncertainty regions about the tip. Right panel: luminosity function of the selected KK 153 RGB stars with superimposed the median model (black line) and the $\pm 1\sigma$ and $\pm 3\sigma$ confidence intervals (dark purple and light purple bands, respectively).

by Lupton (2005)⁹. These absolute magnitudes have been converted in total luminosities in the various passbands assuming the absolute magnitudes of the Sun listed by Willmer (2018)¹⁰.

To convert luminosities into stellar masses we must refer to relations providing the stellar mass-to-light (M/L) ratio as a function of the galaxy colour, as done by Xu et al. (2025). To somehow account for the systematic uncertainty inherent to these relations and to the models they are derived from we decided to derive M/L_g and M/L_r from various relations from different authors. In particular we used the equations as a function of $(g - r)_0$ colour by Herrmann et al. (2016), as done by Xu et al. (2025), by Zibetti et al. (2009), and the two sets of relations derived from different models by Roediger & Courteau (2015), for a total of four different M/L estimates per passband. For the colour of KK 153, $(g-r)_0 = 0.51$, we obtain $M/L_g(M/L_r)$ values ranging from 1.04(1.01) to 1.43(1.39), implying that the uncertainties tied to the adopted M/L are likely as large as 40% and possibly larger. We adopt the average of these four values as our reference M/L and their standard deviation as the associated uncertainty, that is $M/L_g = 1.18 \pm 0.17$, and $M/L_r = 1.20 \pm 0.17$.

From these M/L ratios we get $M_{\star} = 2.5 \pm 0.2 \times 10^6 \ M_{\odot}$ and $M_{\star} = 2.1 \pm 0.3 \times 10^6 \ M_{\odot}$ from L_g and L_r , respectively. As our final best estimate of the stellar mass of KK 153 we take the weighted average of these two values, $M_{\star} = 2.4 \pm 0.2 \times 10^6 \ M_{\odot}$.

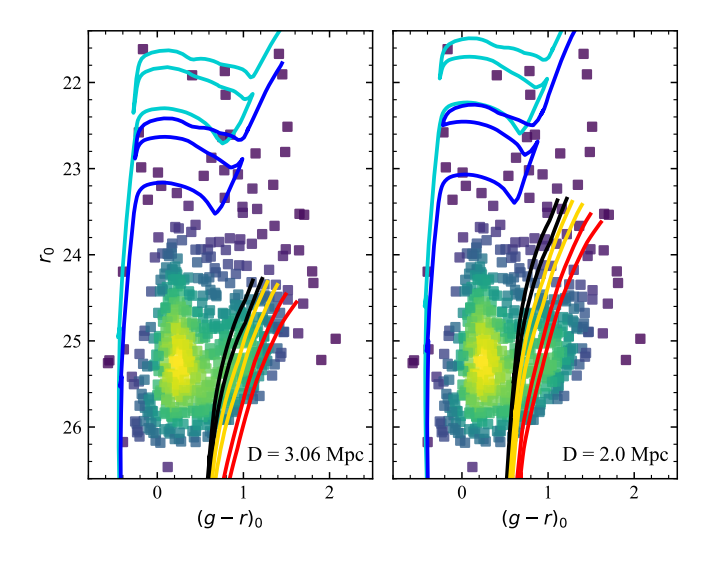


Fig. 7. CMD of KK 153 with isochrones superimposed after correction for the distance measured in this paper (D = 3.06 Mpc, left panel) and for the distance estimated by Xu et al. (2025, D = 2.0 Mpc, right panel). The isochrones displaying the RGB phase have metallicity [M/H] = -2.0 (black), [M/H] = -1.5 (yellow), and [M/H] = -1.0 (red). For each metallicity, isochrones of two different ages are plotted, 5.0 Gyr and 10.0 Gyr, where in each pair the older isochrone is redder than the younger one. Two age ≤ 100 Myr isochrones with [M/H] = -1.0 are also superimposed to both CMDs with the aim of fitting the handful of young KK 153 stars included in our sample. The young isochrones in the left panel have age ≤ 40 Myr (in cyan), and 63 Myr (in blue), in the right panel age ≤ 63 Myr (in cyan), and 100 Myr (in blue).

This is more than five times larger than the estimate by Xu et al. (2025, $M_{\star} = 4.1^{+10.0}_{-2.6} \times 10^5 M_{\odot}$), albeit the statistical difference is less than 2σ , due to the very large size of the upper error bar of the Xu et al.'s value. The most important factor contributing to the difference between the two stellar mass estimates is the improved distance (2.35×), then the brighter integrated magnitudes (1.58×), and finally the difference in M/L value, contributing with a 1.46× factor. The latter difference is due to the bluer colour obtained by Xu et al. (2025), $(g - r)_0 =$ 0.4, instead of our $(g - r)_0 = 0.5$. If our hypothesis of Xu et al. (2025) measuring the integrated magnitude over an aperture smaller than the one adopted here (Sect. 2.2) is correct, it may also explain the difference in colour, since smaller apertures would progressively remove the contribution of red RGB stars to the integrated colour, as these stars populate also the outskirts of the galaxy (and dominate the stellar mass budget), while young blue stars are the prime contributor of light in the central region but are absent outside (and are expected to provide a minor contribution to the mass budget).

4. Discussion and conclusion

We have obtained deep photometry of KK 153, a stellar system recently identified as a local low-stellar-mass gas-rich dwarf galaxy by Xu et al. (2025). Based on a very uncertain distance estimate these authors suggested that KK 153 may be a UFD galaxy at the edge of the Local Group, akin to Leo P (McQuinn et al. 2015). However, our newly derived and much more accurate distance, measured from the RGB Tip, relocates the dwarf clearly beyond the Local Group, leading also to a

https://www.sdss3.org/dr9/algorithms/ sdssUBVRITransform.php#Lupton2005

¹⁰ https://mips.as.arizona.edu/~cnaw/sun.html

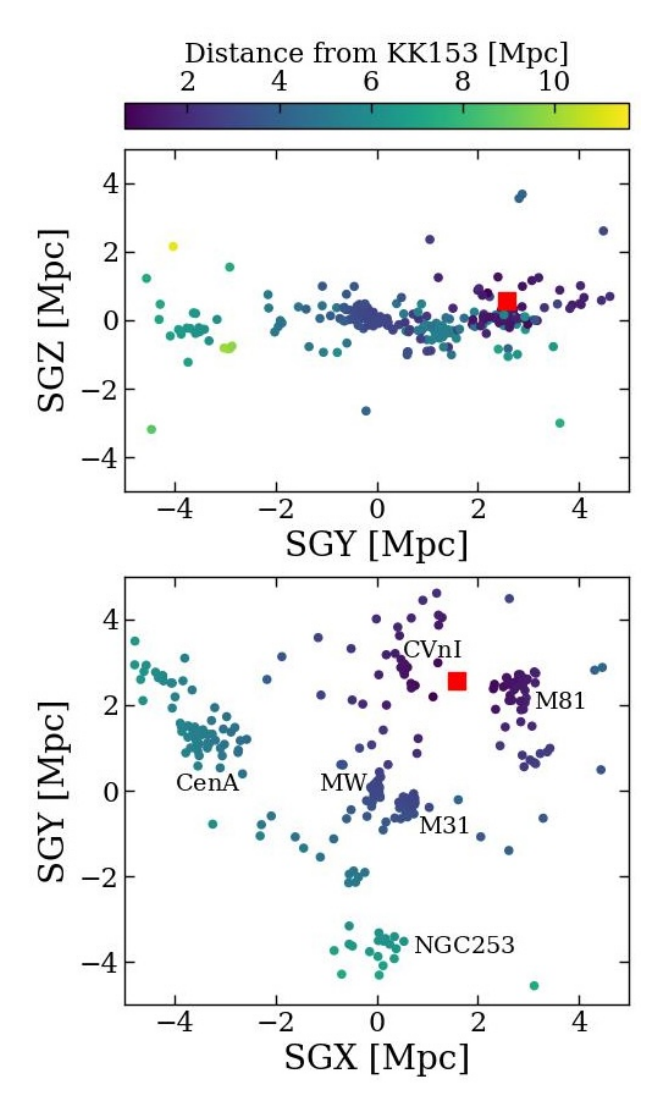


Fig. 8. Location of KK 153 in cartesian Supergalactic coordinates. Upper Panel: SGY-SGZ projection. Lower panel: SGX-SGY projection. KK 153 is plotted as a large red square while the confirmed dwarfs in the P24 catalogue are plotted as small filled circles color-coded according to their distance from KK 153. The main galaxy groups are labelled in the lower panel.

significantly larger stellar mass estimate, significantly beyond the UDF / normal dwarf limit adopted by Xu et al. (2025), $M_{\star} \simeq 10^5~M_{\odot}$. Considering the integrated V luminosity L_V , KK 153 is $\simeq 4.5$ times brighter than Leo P, and $\simeq 14$ times brighter than Leo T (P24). Given the similarity in the stellar content, it can be concluded that KK 153 exceeds these two galaxies by similar factors also in stellar mass.

To properly place KK 153 into the context of local dwarfs, in Fig 9 we show its position within the r_h vs. M_V and $M_{\rm H{\sc i}}$ vs. M_V relations defined by the confirmed dwarf galaxies listed in the P24 catalogue. KK 153 lies on the high surface brightness edge of the luminosity – size relation, as typical of isolated dwarfs (Mutlu-Pakdil et al. 2025), surrounded by galaxies with similar stellar mass. On the other hand, the lower panel of Fig 9 shows that it is indeed among the faintest known dwarfs retaining a measurable amount of H I in the P24 list, displaying a $M_{\rm H{\sc i}}/M_{\star}$ ratio $\simeq 0.5$, quite typical of dwarf galaxies. In this plot there are eleven dwarfs fainter than KK 153, four of them are more distant than it, three are part of the NGC 3109 group (Antlia and Antlia B at D $\simeq 1.3$ Mpc, and Leo P, at D $\simeq 1.6$ Mpc),

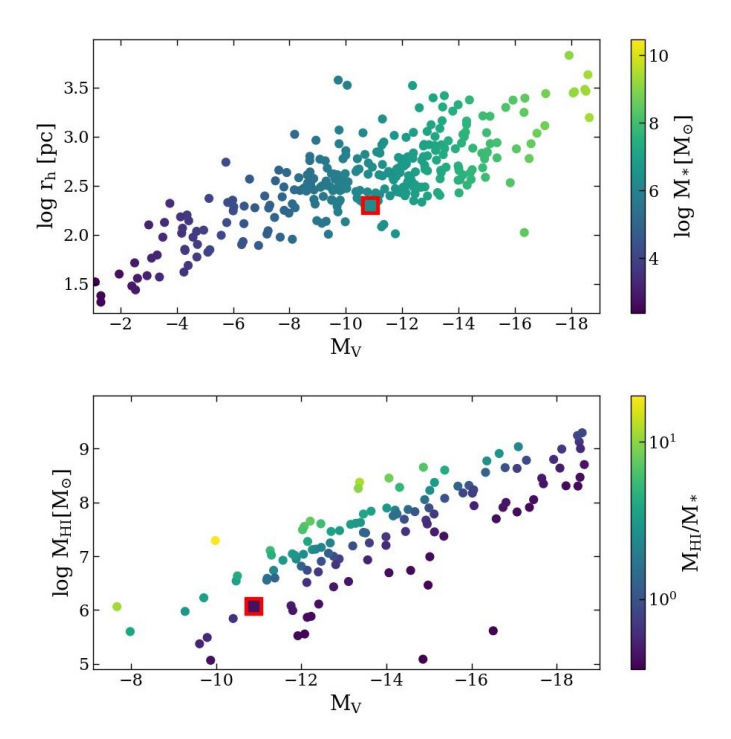


Fig. 9. KK 153 in the context of the confirmed dwarf galaxies in the P24 database. Upper panel: M_V vs. $\log r_h$. Points are colour-coded according to the stellar mass derived from the integrated V luminosity adopting $M/L_V=1.0$ (while in the original P24 list $M/L_V=2.0$ is adopted). Lower panel: M_V vs. $\log M_{\rm H\,\tiny I}$ for the P24 dwarfs having a valid measure of the H I mass. The points are colour-coded according to their H I mass to stellar mass ratio. Also in this case $M/L_V=1.0$ was adopted. In both panels KK 153 is highlighted with a red square.

and the remaining four are genuine Local Group members, the dwarf irregulars LGS 3 and Acquarius, the transition type dwarf Phoenix, and the gas-rich UFD Leo T, all having $D \le 1.0$ Mpc.

In terms of distance, isolation, M_V , ellipticity and size KK 153 is remarkably similar to the recently discovered Corvus A dwarf (Jones et al. 2024), that, however, is more gas-rich, having $M_{\rm H\,I}/M_{\star} \simeq 2.3$ (Mutlu-Pakdil et al. 2025). Both galaxies display a remarkably regular distribution of H I approximately with the same centre as the star distribution (Jones et al. 2024; Xu et al. 2025), in contrast, e.g., with the cases of other similar isolated dwarfs like VV 124(UGC 4879) (Bellazzini et al. 2011) or Pavo (Jones et al. 2025). This variety of H I morphologies may suggest that we are observing these galaxies in different phases of their activity, within a cycle that may include star formation - feedback - gas ejection - gas recovery and resettlement to an equilibrium configuration (see, e.g., Rey et al. 2022; Gutcke et al. 2022; Rey et al. 2024; McQuinn et al. 2024; Jones et al. 2025, and references therein).

In a study aimed at exploring the threshold between galaxies quenched by re-ionisation and survivors that were able to form stars after that phase, Gutcke et al. (2022) performed detailed very high-resolution simulations of five halos in a stellar mass range (at z=0) enclosing KK 153, $0.22\times10^6~M_\odot \le M_\star \le 9.42\times10^6~M_\odot$. They found that, while the onset of re-ionisation heavily impacted the star formation of all the considered haloes, three of them were able to re-ignite the star formation after a period of quiescence, albeit at a much lower rate than before. One of these survivors, their 'HaloD', displays z=0 properties remarkably similar to KK 153 ($M_\star=1.6\times10^6~M_\odot, r_h=120$ pc, ongoing star

formation). It is intriguing to note that one of the Gutcke et al. (2022) haloes that was permanently quenched by re-ionisation, 'HaloC', has both a slightly larger halo mass and stellar mass than 'HaloD', highlighting the delicate interplay of the various factors at play in determining the actual destiny of such small galaxies, not simply total mass (see also McQuinn et al. 2024, for further discussion and references). The study of systems like KK 153 may help us to get insight into this crucial phase of the evolution of dwarf galaxies, and, indeed they have been a subject of intense research in the last decade (see, e.g., Cannon et al. 2011, 2015; McQuinn et al. 2015; Sand et al. 2015b; Hirschauer et al. 2016; McQuinn et al. 2024; Mutlu-Pakdil et al. 2025; Jones et al. 2025, and references therein).

Acknowledgements. The authors thank an anonymous referee for a constructive and useful report. MB, FA and DPM acknowledge financial support to this project by INAF, through the PRIN-2023 grant Ob. Fu 1.05.23.05.09 "Dwarf galaxies as probes of the Lambda Cold Dark Matter hierarchical paradigm at the smallest scales" (P.I.: F. Annibali). This paper is supported by the Italian Research Center on High Performance Computing Big Data and Quantum Computing (ICSC), project funded by European Union - NextGenerationEU and National Recovery and Resilience Plan (NRRP) - Mission 4 Component 2 within the activities of Spoke 3 (Astrophysics and Cosmos Observations). RP acknowledges the support to this study by the PRIN INAF Mini Grant 2022 (Ob.Fu. 1.05.12.04.02 - CUP C33C22000970005). FA acknowledges support by the PRIN INAF Mini Grant 2024 (Ob.Fu.1.05.24.07.02 – CUP C33C24001360005). This work is based on LBT data. The LBT is an international collaboration among institutions in the United States, Italy, and Germany. LBT Corporation partners are the University of Arizona on behalf of the Arizona Board of Regents; Istituto Nazionale di Astrofisica, Italy; LBT Beteiligungsgesellschaft, Germany, representing the Max Planck Society, the Leibniz Institute for Astrophysics Potsdam, and Heidelberg University; the Ohio State University, and the Research Corporation, on behalf of the University of Notre Dame, University of Minnesota, and University of Virginia. We acknowledge the support from the LBT-Italian Coordination Facility for the execution of observations, data distribution, and reduction. This work made use of SDSS-V data. Funding for the Sloan Digital Sky Survey V has been provided by the Alfred P. Sloan Foundation, the Heising-Simons Foundation, the National Science Foundation, and the Participating Institutions. SDSS acknowledges support and resources from the Center for High-Performance Computing at the University of Utah. SDSS telescopes are located at Apache Point Observatory, funded by the Astrophysical Research Consortium and operated by New Mexico State University, and at Las Campanas Observatory, operated by the Carnegie Institution for Science. The SDSS web site is www.sdss.org. SDSS is managed by the Astrophysical Research Consortium for the Participating Institutions of the SDSS Collaboration, including the Carnegie Institution for Science, Chilean National Time Allocation Committee (CNTAC) ratified researchers, Caltech, the Gotham Participation Group, Harvard University, Heidelberg University, The Flatiron Institute, The Johns Hopkins University, L'Ecole polytechnique fédérale de Lausanne (EPFL), Leibniz-Institut für Astrophysik Potsdam (AIP), Max-Planck-Institut für Astronomie (MPIA Heidelberg), Max-Planck-Institut für Extraterrestrische Physik (MPE), Nanjing University, National Astronomical Observatories of China (NAOC), New Mexico State University, The Ohio State University, Pennsylvania State University, Smithsonian Astrophysical Observatory, Space Telescope Science Institute (STScI), the Stellar Astrophysics Participation Group, Universidad Nacional Autónoma de México, University of Arizona, University of Colorado Boulder, University of Illinois at Urbana-Champaign, University of Toronto, University of Utah, University of Virginia, Yale University, and Yunnan University. This research has made use of the SIMBAD database, operated at CDS, Strasbourg, France. This research has made use of the NASA/IPAC Extragalactic Database (NED), which is operated by the Jet Propulsion Laboratory, California Institute of Technology, under contract with the National Aeronautics and Space Administration. We acknowledge the usage of the HyperLeda database (http://leda.univ-lyon1.fr). In this analysis we made use of TOPCAT (http://www.starlink.ac. uk/topcat/, Taylor 2005), APT (https://www.aperturephotometry.org Laher et al. 2012a,b), DAOPHOT II ALLFRAME(Stetson 1987, 1994), Sextractor (Bertin & Arnouts 1996), numpy, astropy, scipy, matplotlib.

References

Adams, E. A. K., Giovanelli, R., & Haynes, M. P. 2013, ApJ, 768, 77
 Ahumada, R., Allende Prieto, C., Almeida, A., et al. 2020, ApJS, 249, 3
 Anand, G. S., Benítez-Llambay, A., Beaton, R., et al. 2025, arXiv e-prints, arXiv:2508.20157

```
Bellazzini, M., Perina, S., Galleti, S., & Oosterloo, T. 2011, A&A, 533, A37
Belokurov, V. 2013, New A Rev., 57, 100
Bertin, E. & Arnouts, S. 1996, A&AS, 117, 393
Bressan, A., Marigo, P., Girardi, L., et al. 2012, MNRAS, 427, 127
Cannon, J. M., Giovanelli, R., Haynes, M. P., et al. 2011, ApJ, 739, L22
Cannon, J. M., Martinkus, C. P., Leisman, L., et al. 2015, AJ, 149, 72
Giallongo, E., Ragazzoni, R., Grazian, A., et al. 2008, A&A, 482, 349
Giovanelli, R. & Haynes, M. P. 2015, A&A Rev., 24, 1
Giovanelli, R., Haynes, M. P., Adams, E. A. K., et al. 2013, AJ, 146, 15
Graczyk, D., Pietrzyński, G., Thompson, I. B., et al. 2020, ApJ, 904, 13
Gutcke, T. A., Pfrommer, C., Bryan, G. L., et al. 2022, ApJ, 941, 120
Herrmann, K. A., Hunter, D. A., Zhang, H.-X., & Elmegreen, B. G. 2016, AJ,
   152, 177
Hirschauer, A. S., Salzer, J. J., Skillman, E. D., et al. 2016, ApJ, 822, 108
Irwin, M. J., Belokurov, V., Evans, N. W., et al. 2007, ApJ, 656, L13
Jones, M. G., Mutlu-Pakdil, B., Sand, D. J., et al. 2023, ApJ, 957, L5
Jones, M. G., Rey, M. P., Sand, D. J., et al. 2025, ApJ, 990, 164
Jones, M. G., Sand, D. J., Mutlu-Pakdil, B., et al. 2024, ApJ, 971, L37
Laher, R. R., Gorjian, V., Rebull, L. M., et al. 2012a, PASP, 124, 737
Laher, R. R., Rebull, L. M., Gorjian, V., et al. 2012b, PASP, 124, 764
Lee, M. G., Freedman, W. L., & Madore, B. F. 1993, ApJ, 417, 553
Leisman, L., Haynes, M. P., Janowiecki, S., et al. 2017, ApJ, 842, 133
Leisman, L., Rhode, K. L., Ball, C., et al. 2021, AJ, 162, 274
Madore, B. F. & Freedman, W. L. 2020, AJ, 160, 170
Makarov, D., Prugniel, P., Terekhova, N., Courtois, H., & Vauglin, I. 2014, A&A,
   570, A13
McQuinn, K. B. W., Newman, M. J. B., Skillman, E. D., et al. 2024, ApJ, 976,
McQuinn, K. B. W., Skillman, E. D., Dolphin, A., et al. 2015, ApJ, 812, 158
Mutlu-Pakdil, B., Jones, M. G., Sand, D. J., et al. 2025, arXiv e-prints,
   arXiv:2509.16307
Pace, A. B. 2024, arXiv e-prints, arXiv:2411.07424
Perina, S., Barmby, P., Beasley, M. A., et al. 2009, A&A, 494, 933
Rey, M. P., Orkney, M. D. A., Read, J. I., et al. 2024, MNRAS, 529, 2379
Rey, M. P., Pontzen, A., Agertz, O., et al. 2022, MNRAS, 511, 5672
Roediger, J. C. & Courteau, S. 2015, MNRAS, 452, 3209
Sacchi, E., Bellazzini, M., Annibali, F., et al. 2024, A&A, 691, A65
Salaris, M. & Cassisi, S. 1998, MNRAS, 298, 166
Sand, D. J., Crnojević, D., Bennet, P., et al. 2015a, ApJ, 806, 95
Sand, D. J., Spekkens, K., Crnojević, D., et al. 2015b, ApJ, 812, L13
Saul, D. R., Peek, J. E. G., & Putman, M. E. 2014, MNRAS, 441, 2266
Schlafly, E. F. & Finkbeiner, D. P. 2011, ApJ, 737, 103
Schlegel, D. J., Finkbeiner, D. P., & Davis, M. 1998, ApJ, 500, 525
Simon, J. D. 2019, ARA&A, 57, 375
Skillman, E. D., Salzer, J. J., Berg, D. A., et al. 2013, AJ, 146, 3
Stetson, P. B. 1987, PASP, 99, 191
Stetson, P. B. 1994, PASP, 106, 250
Taylor, M. B. 2005, in Astronomical Society of the Pacific Conference Series,
   Vol. 347, Astronomical Data Analysis Software and Systems XIV, ed.
   P. Shopbell, M. Britton, & R. Ebert, 29
Willmer, C. N. A. 2018, ApJS, 236, 47
Xu, J.-L., Zhu, M., Yu, N.-P., et al. 2025, ApJ, 982, L36
Zhang, C.-P., Zhu, M., Jiang, P., et al. 2024, Science China Physics, Mechanics,
   and Astronomy, 67, 219511
```

Zibetti, S., Charlot, S., & Rix, H.-W. 2009, MNRAS, 400, 1181

Annibali, F., Beccari, G., Bellazzini, M., et al. 2020, MNRAS, 491, 5101 Bellazzini, M., Beccari, G., Battaglia, G., et al. 2015a, A&A, 575, A126

Bellazzini, M., Magrini, L., Mucciarelli, A., et al. 2015b, ApJ, 800, L15

Bellazzini, M. & Pascale, R. 2024, A&A, 691, A42